Numerical Investigation of the Physical Mechanisms behind Geysers in Storm Sewer Systems: A Slug Analysis Based on a Computational Study of Geyser Eruptions

Abbas Sharifi[1]; Sumit R. Zanje[2]; Pratik Mahyawansi[3]; and Arturo S. Leon[4]

[1]Dept. of Civil and Environmental Engineering, Florida International Univ., Miami.
Email: asharifi@fiu.edu
[2]Dept. of Civil and Environmental Engineering, Florida International Univ., Miami.
Email: szanj001@fiu.edu
[3]Dept. of Mechanical and Material Engineering, Florida International Univ., Miami.
Email: pmahy002@fiu.edu
[4]Dept. of Civil and Environmental Engineering, Florida International Univ., Miami.
Email: arloen@fiu.edu

ABSTRACT

The purpose of this study is to investigate the dynamics of geyser eruptions using three-dimensional computational fluid dynamics in an inverted Tee pipe. The research focuses on assessing the interaction of air-water phases, using numerical simulations based on a finite volume approach in OpenFoam. The geometry of the design includes horizontal 6-in. pipes and a drop shaft along with an air intake. Preliminary results indicate that, during the eruption condition, water and air superficial Reynolds numbers exceed 105 in the horizontal pipe. Furthermore, this study examines how pressure changes influence slug formation and growth in horizontal pipes, as well as the intensities of geysers. Based on our findings, as a result of higher pressure within the slug area, a larger slug causes more intense eruptions. The results of this study provide valuable insight into the fluid dynamics of geyser eruptions in storm sewer systems.

Keywords: Computational Fluid dynamics, geyser, storm sewer system, slug flow, two-phase flow.

INTRODUCTION

Stormwater Geysers, characterized by eruptions of air and water mixture from manholes, present significant risks to safety and property. These phenomena have drawn attention to the need for improved stormwater management in urban planning. Research has shown that air pockets in stormwater systems are a major factor in geyser formation (Shao, 2013). Wright et al. (2009) highlighted the release of large air pockets from dropshafts as a key element in these events. Factors such as manhole cover mobility and size, pipe depth, inflow rate, dropshaft dimensions, and diameter ratios are known to influence the intensity of geysers (Zhang et al., 2022; Choi et al., 2019). Leon (2016) linked geyser intensity to the elevation of the water column in the dropshaft and in 2019, he stated that geyser eruption speeds are limited by the sound speed in an air-water mix. The relationship between the air mass flow rate and geyser height is also significant (Leon et al., 2019).

Computational fluid dynamics (CFD) models have been useful for simulating the pressure oscillations in stormwater systems that can lead to geysers. Wang & Vasconcelos (2020) pointed

out the heightened risk of manhole cover displacement due to sudden releases of air pockets. Li et al. (2023) categorized geysers into air-releasing, rapid-filling, and hybrid types, with the latter influencing the heights of the former two. Equations developed for predicting geyser heights have a reasonable accuracy (within a 15% error margin). Allasia et al. (2023) emphasized the severity of geysers when an entire air pocket reaches a shaft, and Yang & Yang (2023) noted that baffle-drop shaft pressure can fluctuate significantly, leading to hydrodynamic loads much higher than normal discharges. Also, factors such as trapped air volume, ventilation conditions, and upstream water height affect velocity and pressure distribution (Li et al., 2023). Chan (2023) found that downward inflow reduces the upward movement of air pockets, aiding their expulsion. Zhou et al. (2023) developed a model focusing on energy dissipation via transient wall shear stresses and convective heat transfer during air pocket filling. Shao and Yost (2018) concluded that pressure surges are usually the main trigger for geysers. These findings collectively underscore the complexity of geyser formation and the urgent need for effective retrofitting strategies to prevent them. The presence of rapid inflow rates and inadequate ventilation frequently leads to air pocket entrapment, according to Vasconcelos and Wright (2006). Their experimental study demonstrated the importance of system design in mitigating the eruption. Wright et al. (2007) investigated the behavior of air pockets in combined sewer systems. They highlighted the impact of shaft diameter on geyser safety, offering a tangible way to reduce risks associated with geysers. Table 1 presents a summary of the literature review and the main findings related to comprehending the behavior of geyser eruptions.

Table 1: Overview of Research Progress in Understanding Geyser Eruption

Authors	Type	Key Results
Vasconcelos & Wright (2006)	Experimental	1. Air pocket entrapment is prevalent, observed in 76% of experiments. 2. Geometry significantly influences air pocket entrapment; ventilation at "dead ends" is crucial. 3. Strong air pressurization observed with smaller orifices; ventilation area should be ≥1% of pipe cross-sectional area. 4. Inflow rates impact air pocket formation; strong rates expel air, while weaker rates leave an air layer. 5. Optimal ventilation to prevent entrapment may be unfeasible; system design should mitigate air pocket entrapment impacts. 6. Structures should withstand high-frequency pressure peaks from sudden air pocket releases.
Vasconcelos & Chosie (2013)	Experimental	1. Air pocket celerity increases with pocket size. 2. Upward slopes result in higher celerity than horizontal slopes. 3. Inflows enhance observed celerity, with variances at higher flow rates. 4. Air pocket front celerity can be approximated as its quiescent celerity plus water flow velocity. 5. This approximation may overestimate celerity at higher water velocities. 6. Air pockets against water flow experience short-lived

		propagation because of shear effects 7. Scale impacts on air and water flows need deeper understanding, prompting larger and smaller pipeline diameter explorations.
Muller et al. (2017)	Experimental and Numerical	1. Utilized a large-scale PVC apparatus to mimic a stormwater tunnel, observing air pocket release and resultant geysers. 2. Noted the influence of the diameter on water displacement in the apparatus. 3. The CFD model effectively mirrored experimental conditions, with slight discrepancies in pressure measurements. 4. Recognized the importance of understanding air-water interface kinematics for stormwater system design.
Li et al. (2023)	Numerical	- Identified three types of geysers: air-releasing, rapid-filling, and hybrid - Hybrid geysers combine properties of air-releasing and rapid-filling geysers - Developed equations for predicting geyser heights with 15% error - Geyser height influenced by water level, pipe pressure, and shaft diameter
Allasia et al. (2023)	Experimental	- Geysering events are more severe when the entire air pocket is released. - Measurement of pressure heads that is below the grade elevation. - Intensity of geysering was significantly higher compared to prior studies. - Gradual release of air pocket impacted the quality of measurements.
Yang & Yang (2023)	Experimental	- Pressure in shaft fluctuates in geyser eruption. - Geyser caused by high-pressure air release & air-water mixture motion. - Established prediction formula for max geyser height. - Hydrodynamic load during geyser is 10 times normal load on baffles. - Emphasized need for prototype simulations and further tests.
Sun et al. (2023)	Experimental and Numerical	- Three flow regimes in the stepped shape dropshaft corresponded to varying air cavity presence: 1- nappe, 2- transition, and 3- skimming flow. - Nappe flow led to increased standing wave peak, whereas transition flow resulted in wave peak fluctuation. - In skimming flow, the standing wave peak and trough were equal, leading to a near disappearance of the standing wave. - The height of the standing wave peak is affected by factors such as the dimensionless flow discharge rate, the relative height of steps, the angle of step rotation, and the curvature of the dropshaft.

Shao (2013) studied two phases, numerically by integrating the Navier-Stokes equations and the Volume of Fluid (VOF) method. Based on their study, they were able to establish a direct connection between air pocket size, pipe pressurization, and surcharged conditions. Choi et al. (2019) introduced an innovative application of Response Surface Methodology that is helpful for hydraulic engineers to calculate pressures on manhole covers and devise effective preventative measures. Lewis et al. (2011) investigated inertial surges and proposed that stormwater tunnel designs incorporate these insights. As a result of their work, air release mechanisms and water flow dynamics were better understood.

This paper employs 3D computational fluid dynamics to investigate geyser eruptions in an inverted Tee pipe, with a focus on the interaction between air and water and slug formation in pipes. Moreover, the effects of high Reynolds numbers and pressure variations within the pipe on the intensity of geyser eruptions are studied. Additionally, the research is examining Kelvin-Helmholtz instability to enhance the understanding of flow complexity in these systems.

METHODS AND MATERIALS

Mathematical formulation

Mathematical equations are provided that are integral to modeling a geyser eruption, employing a two-phase flow approach that is based on interactions between air and water. The continuity equation ensures the conservation of mass within the flow domain, indicating that any change in the density of the fluid mixture is offset by the flow of momentum. It is complemented by state equations for water and air that link the fluid densities to the pressure and temperature, grounded in the principles of the ideal gas law. Also, mixture density is calculated as a combination of water and air densities, factoring in the volume fraction of water, which introduces a coupling between the phases. where $R = 8.1345\ \frac{J}{mol\ K}$ is the molar ideal gas constant, M represents the molar mass, and T is the temperature in Kelvin.

Continuity:

$$\frac{\partial \rho_m}{\partial t} + \nabla \cdot (\rho_m U) = 0 \tag{1}$$

$$\rho_w = \rho_{w,0} + \frac{p}{R_w T}, \rho_a = \frac{p}{R_a T} \tag{2}$$

$$\rho_m = \alpha \rho_w + (1 - \alpha)\rho_a \tag{3}$$

Momentum:

$$\frac{\partial}{\partial t}(\rho_{\mathrm{m}} U) + \nabla \cdot (\rho_{\mathrm{m}} UU) \quad = \quad -\nabla p_d + \mu_{\mathrm{m}}(\nabla.(\nabla \mathrm{U}) + \frac{1}{3}\nabla(\nabla.\mathrm{U})) + \nabla \rho_{\mathrm{m}} \vec{g} + \vec{F}_{\mathrm{vol}} \tag{4}$$

Heat Transfer:

$$\frac{\partial}{\partial t}(\rho_m T) + \nabla \cdot [\rho_m U T] = \nabla \cdot (\Gamma_{\text{eff}} \nabla T) - \left(\frac{\alpha}{c_{v,a}} + \frac{1-\alpha}{c_{v,w}}\right) \times \left(\frac{\partial \rho_m K}{\partial t} + \nabla \cdot (\rho_m U K) + \nabla \cdot (U p)\right) \quad (5)$$

Two-Phase Flow Transport:

$$\frac{\partial}{\partial t}(\alpha) + U.\nabla\alpha + \nabla.\mathrm{U_c}(1-\alpha) = -\frac{\alpha}{\rho_w}\frac{D\rho_w}{Dt} \quad (6)$$

Based on Newton's second law, the momentum equation encapsulates the fluid's dynamic behavior, including pressure, viscous, and gravitational forces, as well as volumetric forces on the fluid. Moreover, the heat transfer equation is tasked with the conservation of energy in the system, accounting for both convective and conductive heat transfer processes in compressible flow. Where g is the gravitational acceleration, p_d is the dynamic pressure as $p_d = p - \rho_m g y$. μ_m is the kinematic viscosity of the mixture, $c_{v,a}$, $c_{v,w}$ are specific heat capacity of the air and water respectively, Γ_{eff} is the eddy diffusivity and K is the specific kinetic energy from $K = 0.5|U|^2$. Moreover, σ is surface tension between the air and the water. $\vec{F}_{\boldsymbol{vol}}$ in Eq. (4) is surface tension term which is derived by the continuum surface force as illustrated in Eq. (7).

$$\vec{F}_{vol} = \sigma\nabla.\left(\frac{\nabla\alpha}{|\nabla\alpha|}\right)\nabla\alpha \quad (7)$$

In the two-phase flow transport equation, D is the material derivative; and U_c is the velocity compression. Superficial velocity is determined by dividing the volumetric flow rate of a liquid or gas by the total cross-sectional area of the pipeline.

$$U_{sw} = \frac{Q_w}{A_f}, \quad U_{sa} = \frac{Q_a}{A_f} \quad (8)$$

Where U_{sw} is water superficial velocity, U_{sa} is air superficial velocity, Q_w, Q_a are water and air volumetric flowrate, respectively and A_f is pipe cross-sectional area. In this formula $A_f = \pi D^2/4$, where D is the diameter of the pipe.

RESULTS AND DISCUSSION

The geometry of the problem, as illustrated in Figure 1, involves an inverted tree pipe system comprising vertical and horizontal pipes within a control volume. Each pipe has a diameter of 15.2 cm (6 inches). The horizontal pipe extends 51 meters in length, while the vertical pipe, also known as a dropshaft, is 6 meters long (Zanje, 2023). Additionally, there is a cylindrical atmosphere control volume with a 1-meter diameter, intended for observing the spilled air-water mixture after a geyser eruption from the dropshaft. An air tank is positioned 30 meters away from the main pipeline's inlet. In this configuration, air is injected into the water following the establishment of steady-state flow in the pipeline. The entire geometry is discretized using the snappyHexMesh tools from OpenFoam.

In this research, a geyser eruption is modeled using the finite volume method in a turbulence regime using the Reynolds-Averaged Navier-Stokes (RANS) model. The simulation employs governing equations for continuity, momentum, energy transfer, and two-phase flow transport to capture the interactions between air and water phases. The PISO algorithm is used for pressure field correction. Initially, the system reaches a steady state without air injection to establish the natural water level in the dropshaft. Subsequently, air is introduced from a tank into the horizontal pipe, influencing water flow. The water and air inlet velocity are determined from the patches pressure. The atmosphere outlet is modeled with an *inletOutlet* condition, permitting inflow and outflow based on pressure differences, and switches to a fixed value as necessary. The pressure *inletOutletVelocity* boundary condition is applied, specifying pressure and calculating velocity from the normal component of adjacent internal cells. The simulation aims to replicate the physical dynamics of a geyser eruption. The velocities at the water and air inlets are computed from their respective pressure readings, 131.932 kPa for water and 132.061 kPa for air, both at a temperature of 293 K. The volume fraction is set to $\alpha = 1$ for water, indicating the presence of the water phase, and $\alpha = 0$ for air in the second phase. Additionally, the pressures at the atmosphere outlet (dropshaft) and water outlet are set to 101.600 kPa and 131.693 kPa, respectively.

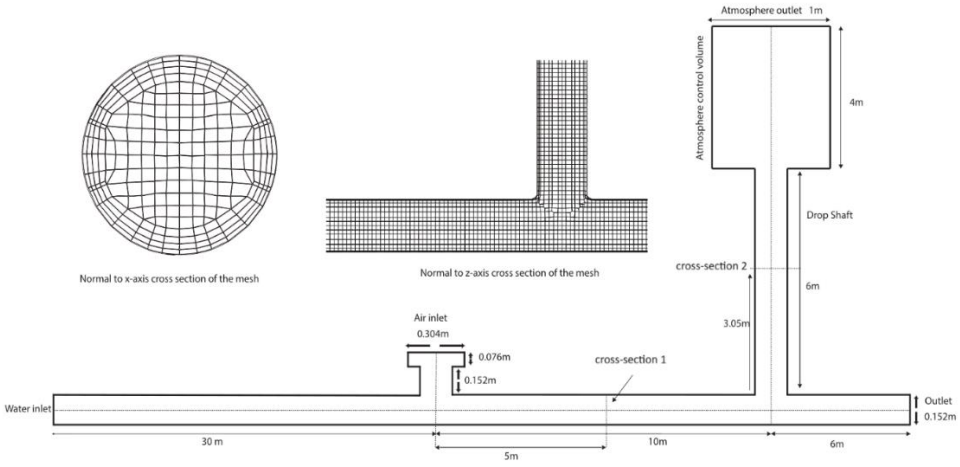

Figure 1. The geometry of the geyser simulation

The initial water level in the dropshaft is set at 3 meters, with the flow direction at this level recorded (as shown in Figure 1, cross-section 2). On cross-section 2, a positive flow direction is termed as an eruption, while a negative flow direction is termed as refilling. Figure 2a presents the eruption flow rate (in liters per second) in the dropshaft at cross-section 2. Therefore, the transition time is divided into seven distinct intervals. Regarding this Figure 2a, three eruption time intervals (Δt_2, Δt_4, Δt_6) and three refilling time intervals (Δt_3, Δt_5, Δt_7) are identified, occurring after air reaches the dropshaft. Each eruption and refilling sequence are considered a cycle in the study. During the 30-second simulation, three cycles are observed. According to Figure 2a, the maximum flow rates of water in cycles 1, 2, and 3 are approximately 5.8 L/s, 3.1 L/s, and 8.8 L/s, respectively. The paper focuses on observing geyser phenomena during the third cycle.

To assess the flow behaviors in each time interval, the superficial Reynolds number of air Re_a and water Re_w are defined as follow (Thaker & Banerjee, 2015):

$$Re_w = \frac{\rho_w U_{sw} D}{\mu_w}, \quad Re_a = \frac{\rho_a U_{sa} D}{\mu_a} \tag{9}$$

Figure 2b in the study presents the superficial Reynolds numbers of water (Re_w) and air (Re_a) at cross-section 1. In this figure, the eruption and refilling phenomena are represented by black and red lines, respectively. The results indicate that during the eruption phase, both Re_w and Re_a are typically above 10^5. Moreover, during the eruption, the process unfolds such that the superficial velocity of water dramatically increases, surpassing that of air. This is observable in Figure 2c. According to this plot, a significant increase in Re_w coupled with a sudden drop in Re_a reached to the maximum eruption points. The maximum eruption points for the three cycles are also illustrated in Figure 2b. Moreover, the point that Re_w equals Re_a can be identified as the eruption time. It is evident that more intense eruptions correspond to higher values of Re_w. This correlation provides an insight into the dynamics of the geyser eruption, emphasizing the relationship between the superficial velocities of water and air and their impact on the intensity of the eruption. In this paper the maximum Re_w for cycles 1,2 and 3 are 3.45×10^5, 2.21×10^5 and 8.31×10^5.

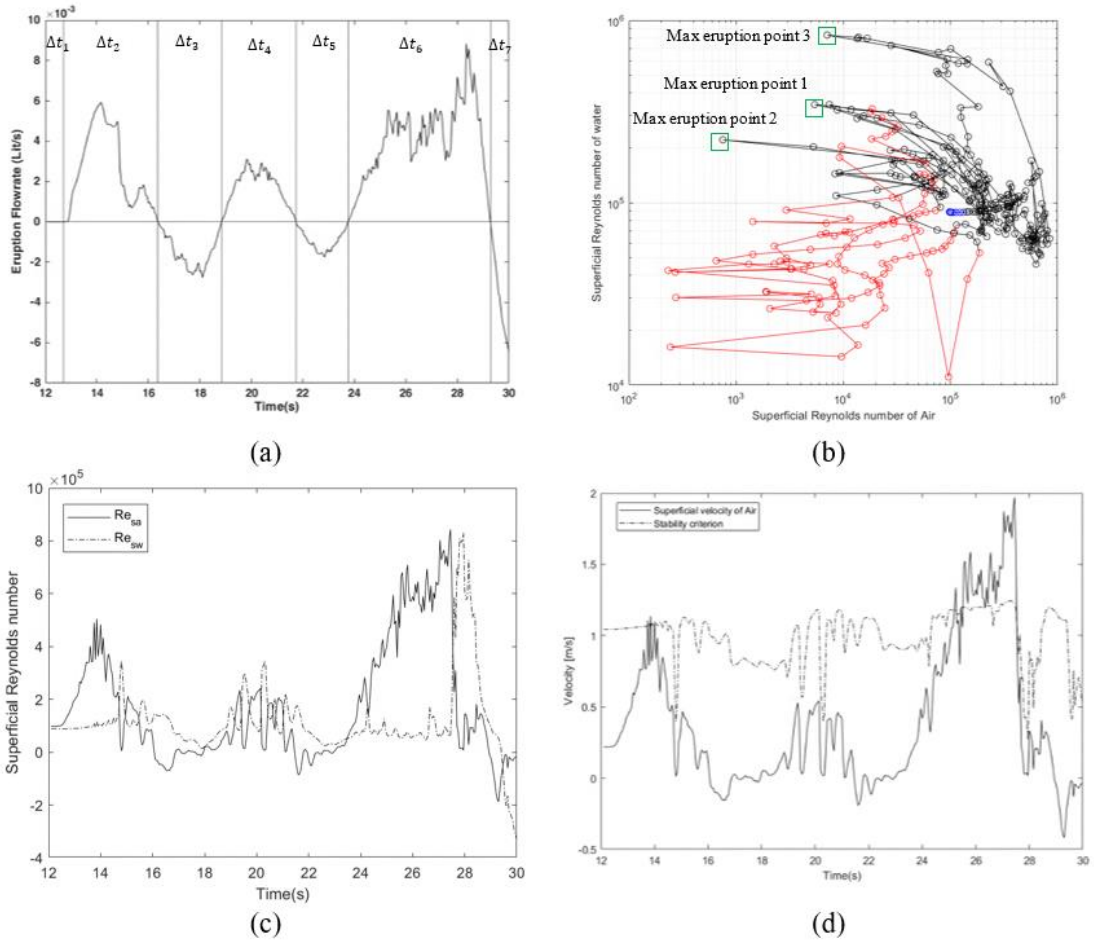

Figure 2. a) The eruption Flow rate of water in cross-section 2 of the dropshaft, b) Superficial Reynolds number of water versus air, c) Superficial Reynolds number over time, d) Stability criteria over time

To study of the in-viscous Kelvin Helmholtz stability in the geyser eruption we used Wallis and Dobson (1973) criteria as follows:

$$V_a = \frac{1}{2}\left[\frac{g(\rho_w - \rho_a)h_a}{\rho_a}\right]^{\frac{1}{2}} \quad (10)$$

Where h_a refers to the distance between the upper wall and the equilibrium water level. This distance is calculated based on the equilibrium level of air in the pipe when the flow is stratified in time interval Δt_1. According to the analysis, when the actual air velocity (V_a) exceeds the superficial air velocity (U_{sa}), there is instability in the flow at cross-section 1. This observation is supported by Figure 2d, which indicates that in-viscous Kelvin-Helmholtz instability occurred in the horizontal pipe during cycles 1 and 3. This type of instability typically arises when there is a velocity difference across the interface between air and water. To gain a deeper understanding of the flow phenomena in the horizontal pipe, the study specifically focuses on the slug flow that occurred in cycle 3. A slug flow occurs when large bubbles of gas, known as slugs, move through a liquid-filled pipe. Pressure, flow rate, and turbulence can all be significantly impacted by this phenomenon. A study of this slug flow is intended to provide insights into the complex interactions and instabilities that occur during the eruption process of a geyser.

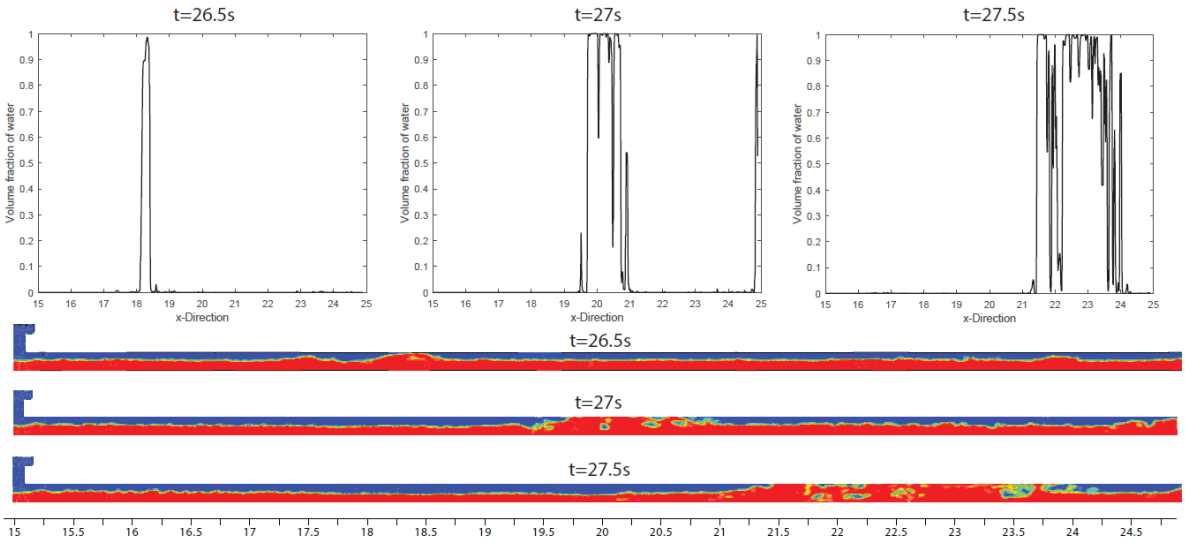

Figure 3. Slug analysis in horizontal pipe between air tank and dropshaft in cycle 3 (eruption)

Figure 3 illustrates the process of slug generation and growth in the horizontal pipe between the air tank and dropshaft during the third cycle of eruption. To visualize this process, a line is plotted at the equilibrium air level inside the pipe. The volume fraction of water is then graphed along this line. As per the observations from Figure 3, the slug begins to form at t=26.5s and continues to grow until t=27.5 s. This development is evident in the contour plot of the water volume fraction. By examining the equilibrium air level line and its intersection with water, the leading and trailing edges of the slug are defined, as depicted in Figure 4a.

Additionally, the distance between the slug's leading and trailing edges is defined as the slug length (L_s). An important observation made in the study is that the pressure within the slug area is higher than in other regions of the flow. This pressure differential is a crucial factor in understanding the dynamics of slug flow, as it influences the behavior and movement of the slug within the pipe.

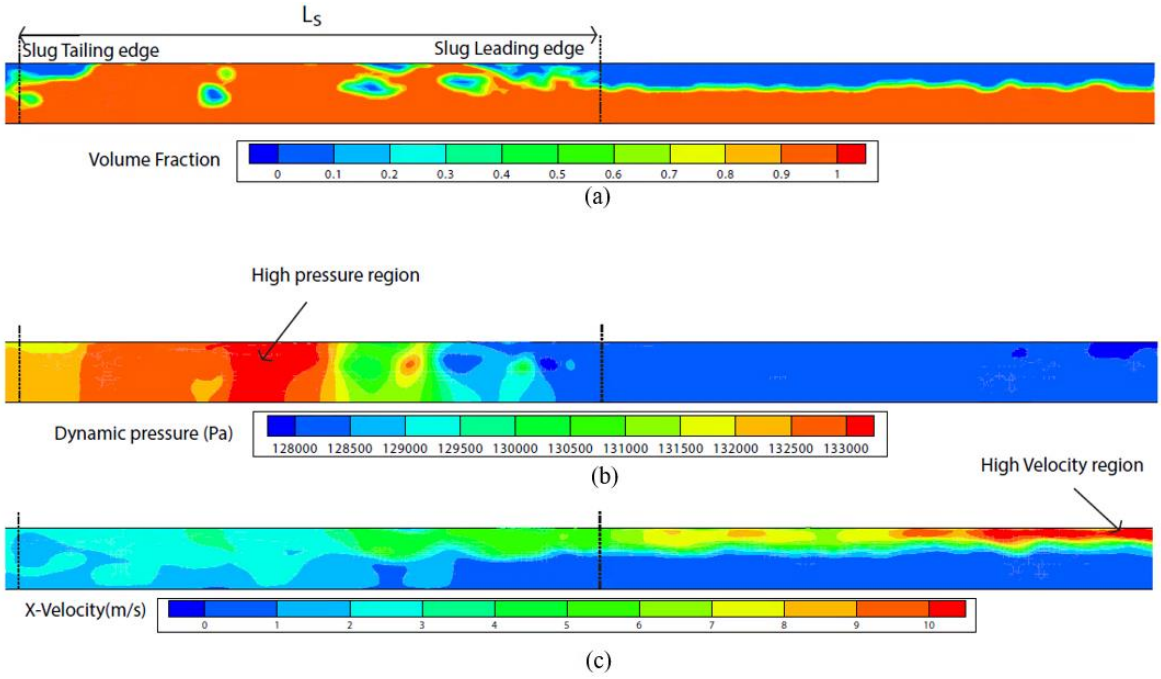

Figure 4. a) Definition of Slug flow length b) Pressure contour around slug and c) Velocity contour around slug

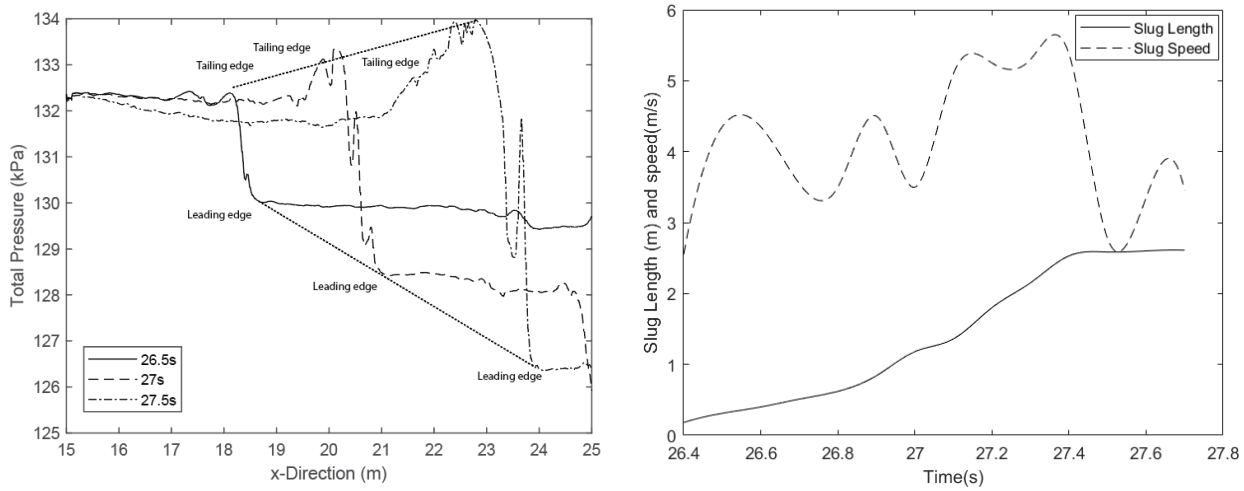

Figure 5. a) Pressure value in slug movement over equilibrium air level line b) The variation of Slug speed and length over time

This study examines the behavior of slugs by plotting pressure values along the equilibrium air level line shown in Figure 5a. This figure reveals that the pressure behind the slug's trailing edge is lower than at its center. Additionally, there is a dramatic drop in pressure in front of the slug's leading edge. This pattern is consistent across all plotted time steps. Interestingly, while the pressure in tailing edge of the slug remains relatively constant, the pressure at the leading-edge decreases as the slug grows. Simultaneously, the maximum pressure within the slug increases over time, correlating with its growth. It is observed that larger slugs have a higher-pressure gradient between their head and tailing edge. When this gradient reaches the dropshaft, a geyser eruption occurs, significantly increasing the pressure and causing water to spill from the dropshaft. The study also tracks the location of the maximum pressure point within the slug over time, enabling the calculation of the slug's speed, as depicted in Figure 5b. The slug's speed also increases over time, though with noticeable fluctuations. In addition to speed, the distance between the slug's leading and trailing edges—its length—is plotted over time. The results demonstrate that the slug's length increases over time, indicating continual growth of the slug. These observations provide crucial insights into the dynamics of slug flow in the horizontal pipe, particularly regarding the relationship between pressure distribution, slug size, and the resultant geyser eruptions.

CONCLUSION

This paper attempts to understand the dynamics and behavior of geyser eruptions in storm sewer systems by applying a CFD model to a simplified piping system consisting of a horizontal pipe and a vertical pipe (inverted Tee). The primary objective is to understand the complex interactions of air - water phases preceding and during geyser eruptions and to identify the key factors influencing these events. Utilizing the finite volume method using OpenFoam, the study simulates a system comprising vertical and horizontal pipes, focusing on the dynamics of slug flow and pressure variations within the inverted Tee. The preliminary simulation carried out over a 30-second period, reveals three distinct cycles of eruption and refilling. Each cycle exhibits characteristics in terms of flow rates and behaviors. The initial finding indicate that both the water and air Reynolds numbers exceed 10^5 during eruptions. The study charts the generation and growth of a slug in the horizontal pipe, marking significant changes in pressure and flow rates. This slug formation is closely linked to the occurrence and intensity of geyser eruptions. Further analysis shows that the pressure within the slug area increases over time, correlating with its growth. Larger slugs, characterized by higher pressure gradients, are found to trigger more intense eruptions. It will be necessary to expand upon these preliminary findings by utilizing more comprehensive models and empirical data in the future.

FUNDING

The authors gratefully acknowledge the financial support of the National Science Foundation (NSF) under Grant number 1928850. The views expressed are solely those of the authors. NSF does not endorse any products or commercial services mentioned.

REFERENCES

Allasia, D. G., Böck, L. É., Vasconcelos, J. G., Pinto, L. C., Tassi, R., Minetto, B., and Pachaly, R. L. (2023). Experimental Study of Geysering in an Upstream Vertical Shaft. *Water*, 15(9), 1740.

Chan, S. N. (2023). Air Pocket Expulsion from a Submerged Dropshaft with Inflow. *Journal of Irrigation and Drainage Engineering*, 149(3), 06022010.
Choi, S., Hong, S. H., and Lee, S. O. (2019). Practical Approach to Predict Geyser Occurrence in Stormwater Drainage System. *KSCE Journal of Civil Engineering*, 23, 1108-1117.
Leon, A. S. (2016, May). New evidence on the causes of explosives geysers in stormwater and combined sewer systems: A simplified model for the prediction of these geysers. In *World environmental and water resources congress 2016* (pp. 224-233).
Leon, A. S. (2019). Mechanisms that lead to violent geysers in vertical shafts. *Journal of Hydraulic Research*, 57(3), 295-306.
Lewis, J., Wright, S. J., and Vasconcelos, J. (2011). Mechanisms for surges in vertical shafts in stormwater tunnels. *Journal of Water Management Modeling*.
Li, X., Zhang, J., Zhu, D. Z., and Qian, S. (2023). Modeling geysers triggered by an air pocket migrating with running water in a pipeline. *Physics of Fluids*, 35(4).
Muller, K. Z., Wang, J., and Vasconcelos, J. G. (2017). Water displacement in shafts and geysering created by uncontrolled air pocket releases. *Journal of Hydraulic Engineering*, 143(10), 04017043.
Shao, Z. S. (2013). *Two-dimensional hydrodynamic modeling of two-phase flow for understanding geyser phenomena in urban stormwater system*. University of Kentucky.
Shao, Z. S., and Yost, S. A. (2018). Numerical investigation of driving forces in a geyser event using a dynamic multi-phase Navier–Stokes model. *Engineering Applications of Computational Fluid Mechanics*, 12(1), 493-505.
Sun, J., Qian, S., Xu, H., Chen, Y., and Ren, W. (2023). Standing waves of the stepped dropshaft in a deep tunnel stormwater system. *Water Science and Technology*, 87(2), 407-422.
Thaker, J., and Banerjee, J. (2015). Characterization of two-phase slug flow sub-regimes using flow visualization. *Journal of Petroleum Science and Engineering*, 135, 561-576.
Vasconcelos, J. G., and Wright, S. J. (2006). Mechanisms for air pocket entrapment in stormwater storage tunnels. In *World Environmental and Water Resource Congress 2006: Examining the Confluence of Environmental and Water Concerns* (pp. 1-10).
Vasconcelos, J., and Chosie, C. D. (2013). Kinematics of entrapped air pockets within stormwater storage tunnels. *Journal of Water Management Modeling*.
Wang, J., and Vasconcelos, J. G. (2020). Investigation of manhole cover displacement during rapid filling of stormwater systems. *Journal of Hydraulic Engineering*, 146(4), 04020022.
Wright, S. J., Lewis, J. W., and Vasconcelos, J. G. (2009). Physical processes resulting in geyser formation in rapidly filling stormwater tunnels. In *World Environmental and Water Resources Congress 2009: Great Rivers* (pp. 1-10).
Wright, S. J., Lewis, J., and Vasconcelos, J. (2007). Mechanisms for stormwater surges in vertical shafts. *Journal of Water Management Modeling*.
Yang, Q., and Yang, Q. (2023). Experimental investigation on the hazard of geyser created by an entrapped air release in baffle-drop shafts. *Scientific Reports*, 13(1), 7953.
Zanje, S. R. (2023). *Sewer Geyser Mechanism and Mitigation Strategies* [Doctoral dissertation, Florida International University, Miami, FL].
Zhang, Y., Chen, Y., Qian, S., Xu, H., Feng, J., and Wang, X. (2022). Experimental study on geysers in covered manholes during release of air pockets in stormwater systems. *Journal of Hydraulic Engineering*, 148(5), 06022003.
Zhou, L., Lu, Y., Karney, B., Wu, G., Elong, A., and Huang, K. (2023). Energy dissipation in a rapid filling vertical pipe with trapped air. *Journal of Hydraulic Research*, 61(1), 120-132.